J MATER SCI **41** (2006) 4205–4213

Microstructure and ionic conductivity of Sr- and Mg-doped $LaGaO_3$

N. LIU, M. SHI*, C. WANG, Y. P. YUAN
Department of Materials Science and Engineering, Hefei University of Technology, Hefei 230009, People's Republic of China
E-mail: shimin@mail.hf.ah.cn

P. MAJEWSKI, F. ALDINGER
Max-Planck-Institute for Metals Research, Stuttgart, 70569, Germany

Published online: 15 May 2006

Samples of Sr- and Mg-doped $LaGaO_3$ (LSGM) with various concentrations of Sr and Mg were prepared by using solid-state reaction method. Results show that ionic conductivities increase with the increase of relative densities. It can also be known that the optimized concentration in $La_{1-x}Sr_xGa_{1-y}Mg_yO_{3-0.5(x+y)}$ with high conductivity is LSGM1520 or LSGM2015. The results also show that, in various concentrations of LSGM, equiaxed, rode-like, polygonal secondary phases such as $LaSrGaO_4$ or $LaSrGa_3O_7$ were detected besides (La,Sr)(Ga,Mg)O_3 by means of SEM and EDX. With the increase of doped elements, i.e. $x + y$, the grain size increases.

1. Introduction

SOFCs convert chemical energy of a fuel gas directly into electrical work, with great current density and transformation efficiency (more than 50%), and are environmentally clean without corrosion and leakage of liquid electrolyte. So they have been widely used in many fields [1–5]. The key materials for SOFCs are solid electrolytes. Yttria-stabilized zirconia (YSZ), as it is well known, is the most widely used solid electrolyte in SOFCs, because of its attractive ionic conductivity at higher temperature, stability in dual environment (oxidizing and reducing) and stability against the electrode materials [3]. But ionic conductivity of YSZ decreases quickly with the decrease of the working temperature [6, 7]. So it must be used at higher temperature. This leads to degeneration when used for a long time and the joint materials for SOFC being oxidized and reduced at high temperature and under oxidizing and reducing atmosphere. Therefore, many scientists are much more interested in the ways to lower the temperature of SOFCs [8]. Sr- and Mg-doped $LaGaO_3$, first synthesized by Ishihara [9] and Goodenough [10], appears high promising as a new solid electrolytes for use at intermediate temperature [11]. The oxide ionic conductivity of $La_{1-x}Sr_xGa_{1-y}Mg_yO_{3-0.5(x+y)}$(LSGM) is around 0.10 S/cm at 800°C (comparable to that of yittria- stabilized zirconia at 1000°C) [12]. It has negligible electronic conduction at temperature lower than 800°C and a stable performance over long operating time [12]. These superior electrical and chemical properties appear to make it the leading new generation material for use as a solid electrolyte in SOFCs operating at or below 800°C [13]. It was reported that the synthesis of LSGM without secondary phase was found to be rather difficult [13–16], the secondary phases such as $LaSrGaO_4$,$LaSrGa_3O_7$,$La_4Ga_2O_9$ or $LaGa_2O_4$, appeared easily. Goodenough *et al*. investigated the synthesis of LSGM powders by Sol-gel method [17]. Tarancon *et al*. investigated the synthesis of LSGM powders by acrylamide polymerization [18]. Cong *et al*. investigated the synthesis of LSGM powders by glycine-nitrate combustion method [19]. Baskaran *et al*. investigated mechanical properties of LSGM [20, 21], the results show that the addition of 2 wt% Al_2O_3 could increase the bending strength effectively. The systematic works about this materials on phase relationships, ion conductivity, microstructures and testing of single cells were done by Goodenough *et al*. [22–24]. It was found that the structure of LSGM is cubic, while Lerch and Yao reported that the structure of LSGM is orthorhombic [25, 26] by means neutron scattering and Raman spectroscopy methods. It was found that higher conductivity was found if LSGM was composed of cubic perovskite, the conductivity of LSGM would be decreased quickly if there exist secondary phases [22]. However, the systematic works on the microstructures of this material, especially the effect

*Author to whom all correspondence should be addressed.
0022-2461
DOI: 10.1007/s10853-006-6309-1

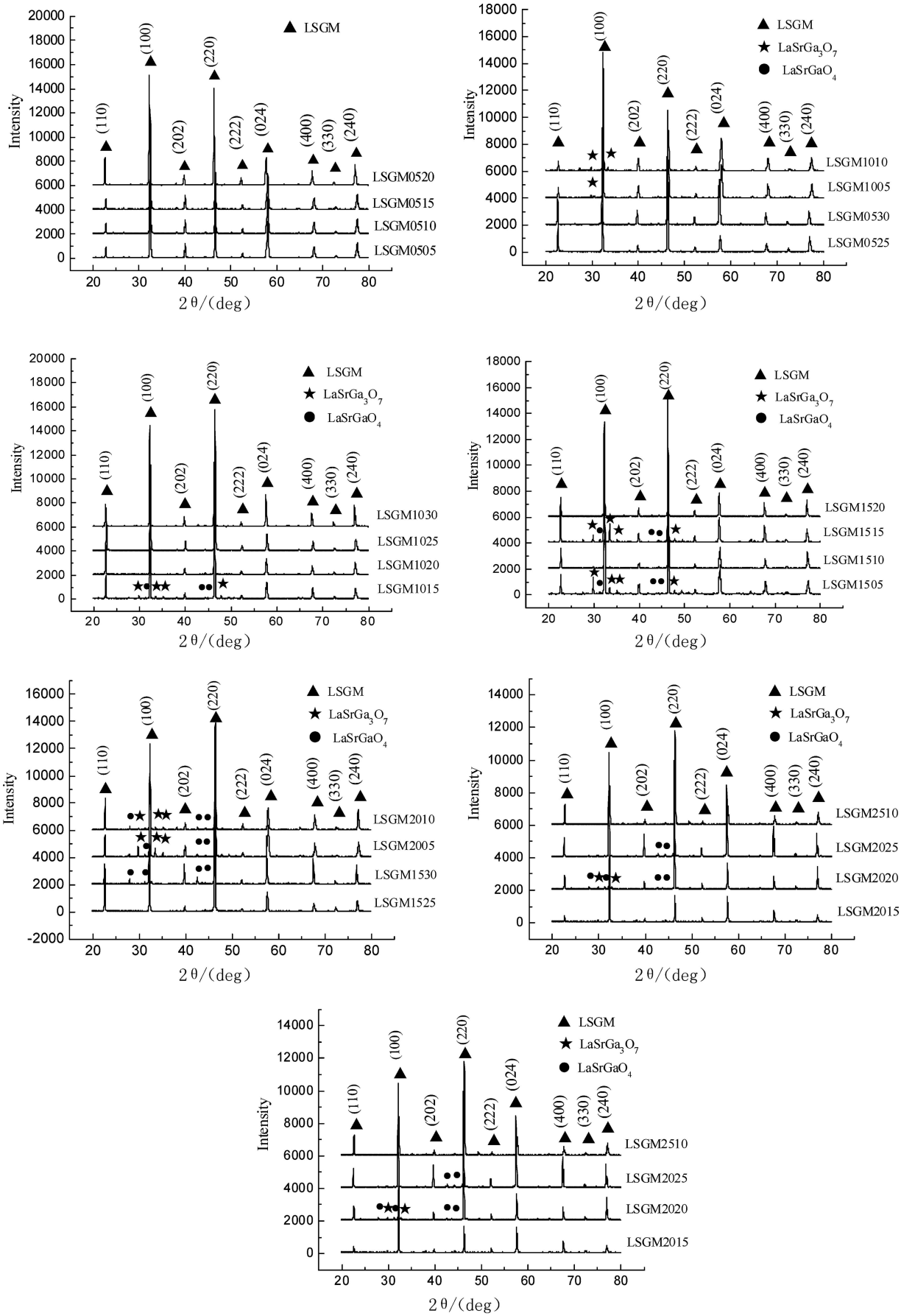

Figure 1 X-ray diffraction patterns of LSGM with various concentrations of Sr and Mg.

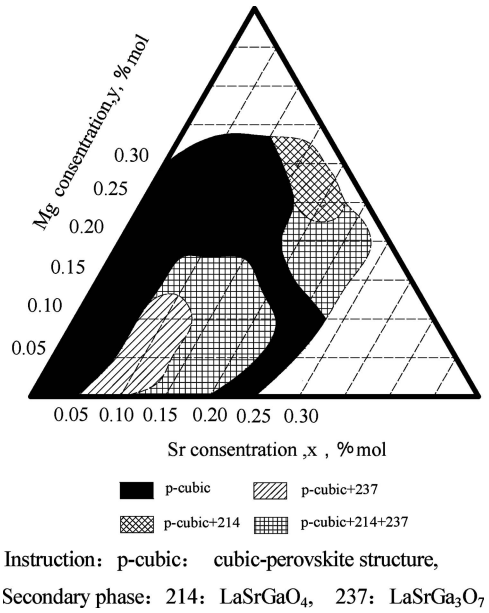

Figure 2 Phase region diagram of LSGM with various concentrations of Sr and Mg.

of the chemical compositions on the microstructure, have not been reported. The purpose of this study is to investigate the relationship between the chemical composition, phase structure, microstructure and ionic conductivity, especially to aim at these secondary phases appeared in the microstructure, in order to provide a better basis for the application of LSGM in SOFCs.

TABLE I Effect of sintering time on densities of LSGM1520

Sintering technology	Relative density(%)
1500°C holding 6 h	93.3
1500°C holding 12 h	95.6
1500°C holding 24 h	97.5
1500°C holding 36 h	95.4

2. Experimental

LSGM samples various concentrations of Sr and Mg were prepared by means of solid-state reaction method. La_2O_3 (purity 99.99%, Aldrich Chemical Company, Inc Miwaukee, USA), $SrCO_3$ (purity 99%, Aldrich chemical CO., Ltd. Gillingham, dorset-England), Ga_2O_3 (purity 99.99% Sigma-Aldrich chemie Gmbh, Steinheim, Germany) and MgO (purity 99.99%, MERck KGaA, Darmstadt, Germany) were used as starting powders. In order to obtain LSGM with various x, Sr concentrations and y, Mg concentrations ($0.05 \leq x \leq 0.25$, $0.05 \leq y \leq 0.30$), every starting powders were put into nylon pot after weighed with the high accuracy analytical balance by stoichiometric proportion, mixed with ZrO_2 ceramic ball and appropriate amount of absolute alcohol and then grinded for 2 h in planetary ball mill (rotation speed, 100 r/min) to get slurries. The slurries were desiccated in desiccator and then abraded in an agate abrasive bowl. The abraded powders in a ceramic vessel were heated to 1200°C in a 5 kw box electronic furnace at a heating rate 1°C/min, heat-preserved for 24 h, calcined and furnace-cooled, then calcined again with the same

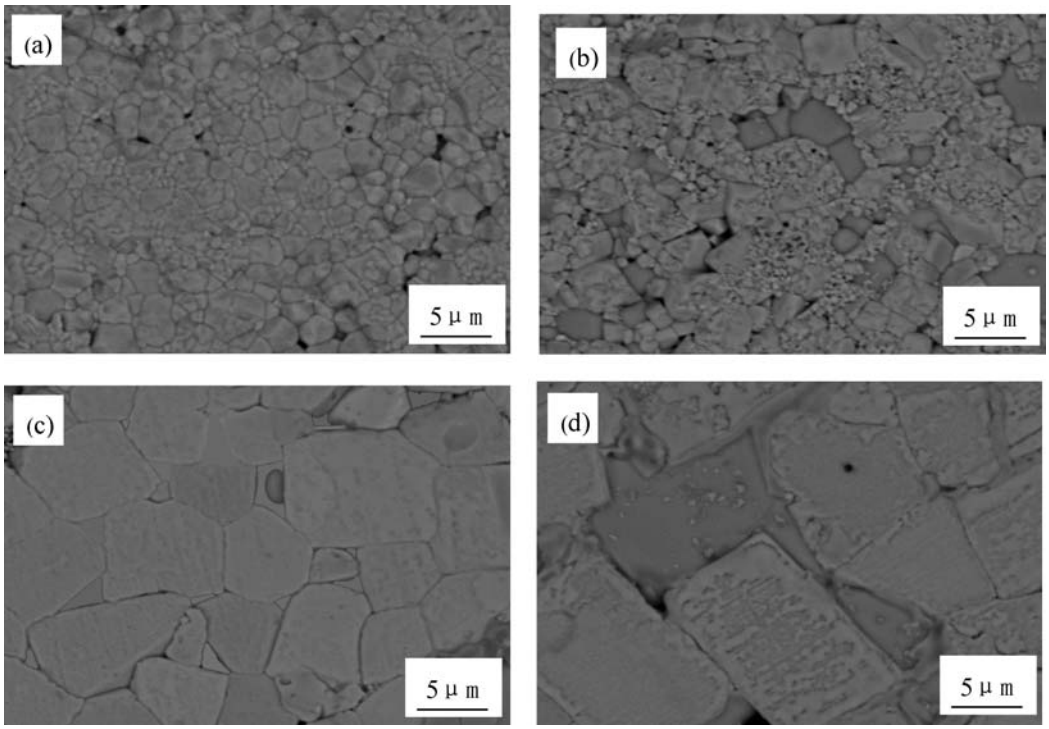

Figure 3 Typical back-scattered SEM micrograph of LSGM1520 sintered at 1500°C for different times. (a) 1500°C × 6 h, (b) 1500°C × 12 h, (c) 1500°C × 24 h, (d) 1500°C × 36 h.

technology. The sintered powders were prilled by using solution of polyvinyl alcohol water solution as plastizer, uniaxially pressed at 170 MPa, then degreased and pre-sintered to 900°C and finally sintered at 1500°C for 24 h at a heating rate 0.5°C/min. In order to denote the effect of sintering time on the density and microstructure, the LSGM1520 was sintered at 1500°C for 6, 12, 24 and 36 h at a heating rate 1°C/min, respectively.

The densities of sintered samples were measured by using the Archimedes water immersion method. The phase structures of starting powders and sintered samples were analyzed by D/max-rB (Rigaku CO., Ltd, Japan, using Cu Kα radiation), X-ray diffractometer (XRD). The microstructures of sintered samples were observed by XL30-ESEM (Germany), scanning electron microscope (SEM). The chemical compositions of some typical microstructures were analyzed by an X-ray energy-dispersive spectrometer (EDX) attached to SEM. The ionic conductivities were measured in air as a function of temperature by using a four-probe impedance spectroscopy. In this method, a small DC potential was applied to electrolyte samples $\sim$13 mm in diameter and 4 mm in thickness, to which platinum electrodes had been applied. In this paper, Sr- and Mg-doped $LaGaO_3$ ceramics with various Sr and Mg additions ($La_{1-x}Sr_xGa_{1-y}Mg_yO_{3-0.5*(x+y)}$) are refer to as LSGM100x100y. For example, LSGM1015 means $La_{0.9}Sr_{0.1}Ga_{0.85}Mg_{0.15}O_{2.875}$.

3. Results and discussion

3.1. XRD

The XRD patterns of 27 kinds of compositions of LSGM are shown in. Fig. 1. The detailed results are shown in Fig. 2. It can be seen that there exist regions of single-phase, two-phase or three-phase in Sr- and Mg-doped

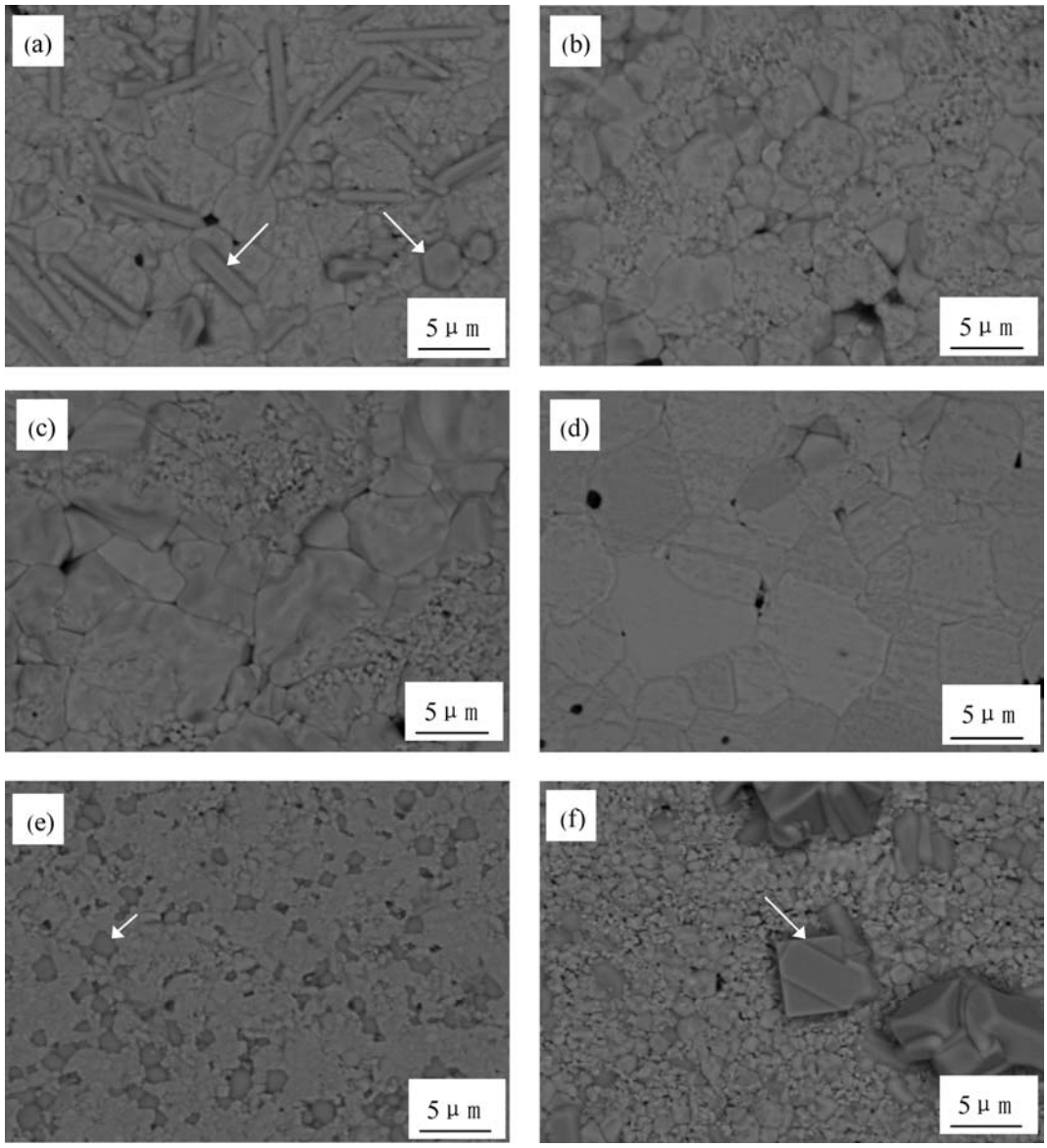

Figure 4 Typical back-scattered SEM micrograph of various LSGM. (a) LSGM0510, (b) LSGM 0515, (c) LSGM0520, (d) LSGM 0525, (e) LSGM1005, (f) LSGM1010, (g) LSGM1020, (h) LSGM1030, (i) LSGM1510, (j) LSGM1515, (k) LSGM1525, (l) LSGM1530, (m) LSGM2015, (n) LSGM2020, (o) LSGM2025, (p) LSGM2510.

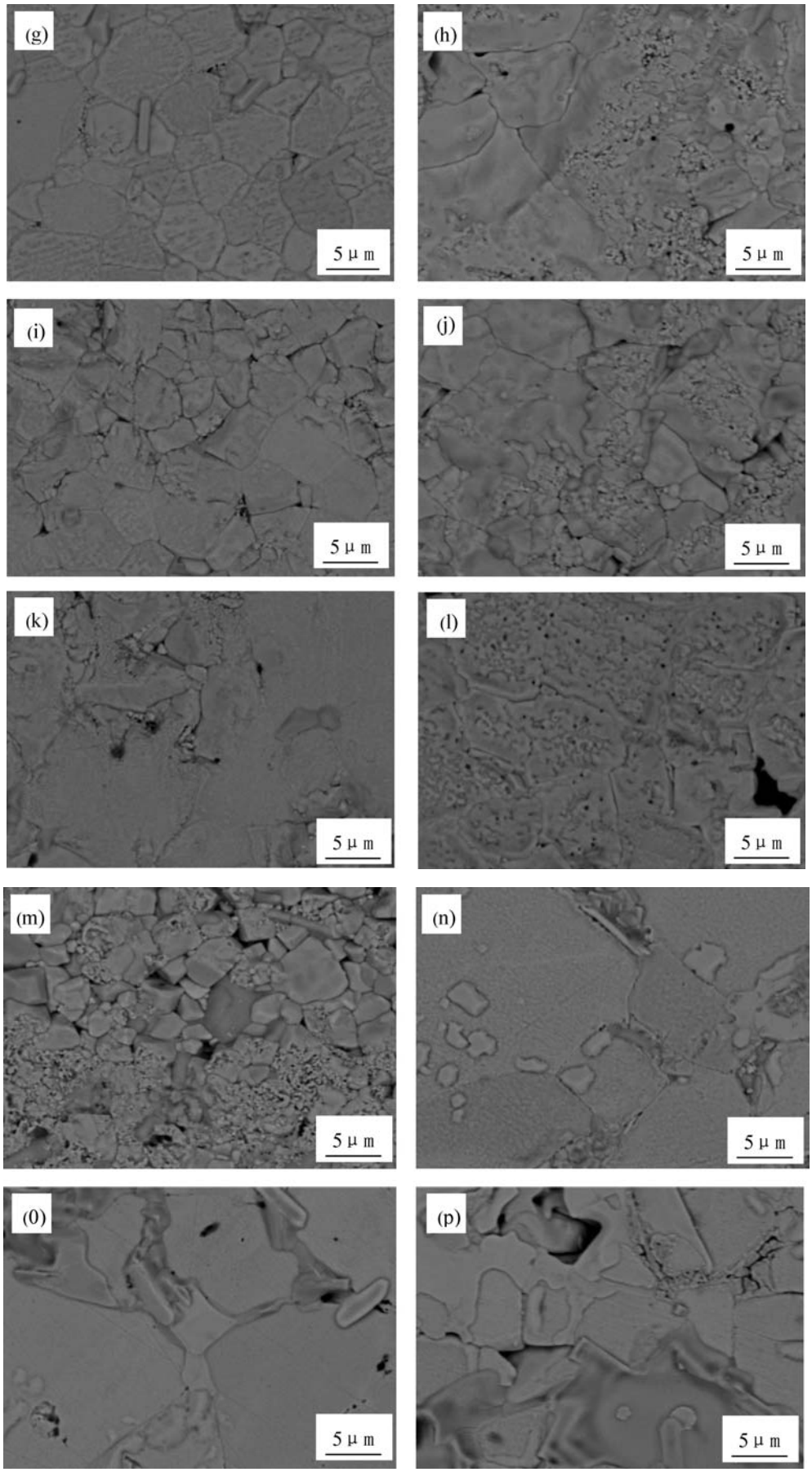

Figure 4 Continued.

$LaGaO_3$. This depends on different compositions of Sr and Mg. In single-phase region, samples of various compositions of LSGM electrolytes are composed of only cubic perovskite-$LaGaO_3$. While in two-phase region or in three-phase region, there exist secondary phases such as $LaSrGrO_4$ or $LaSrGr_3O_7$ besides $LaGaO_3$.

3.2. Relative densities

Effect of sintering time on relative density sintered samples is shown in Table I and Fig. 3. It can be seen that relative densities are increased when sintering time varies from 6 to 24 h. When over sintered sintering time is greater than 24 h (over sintered), as shown in Fig. 3, the grains will grow continuously, cavities at interface of matrix and secondary phase will increase,and Ga will volatilize [27]. It is generally known that oversintring cause lower densities.

TABLE II EDX analysis results of part microstructure of Fig. 4

EDAX ZAF Qualification (Standardless) Element Normalized Element	Wt%	At%	*K*-ratio	*Z*	*A*	*F*
(a) Chemical composition of secondary phase matrix phase in LSGM0510						
OK	18.33	59.11	0.0841	1.2500	0.3668	1.0002
GaL	19.14	14.16	0.0910	0.9938	0.4782	1.0005
MgK	0.34	0.71	0.0013	1.1907	0.3309	1.0011
SrL	13.42	7.90	0.0825	0.9563	0.6450	1.0012
LaL	48.77	18.11	0.4297	0.8726	1.0097	1.0000
Total	100.00	100.00				
(b) Chemical composition of matrix phase in LSGM0510						
OK	15.41	53.85	0.0801	1.2635	0.4114	1.0003
GaL	27.70	22.21	0.1302	1.0043	0.4681	1.0001
MgK	0.33	0.77	0.0012	1.2033	0.2956	0.0004
SrL	1.71	1.09	0.0098	0.9683	0.5923	1.0013
LaL	54.84	22.07	0.4912	0.8831	0.0141	1.0000
Total	100.00	100.00				
(c) Chemical composition of secondary phase in LSGM1005						
OK	15.64	50.06	0.0621	1.2362	0.3210	1.0005
GaL	41.12	30.21	0.2478	0.9831	0.6124	1.0007
MgK	0.00	0.00	0.0000	1.1781	0.3271	1.0012
SrL	17.59	10.28	0.1065	0.9408	0.6430	1.0006
LaL	25.65	9.45	0.2218	0.8590	1.0069	1.0000
Total	100.00	100.00				
(d) Chemical composition of matrix phase in LSGM1005						
OK	15.77	34.13	0.0804	1.2589	0.4048	1.0003
GaL	30.64	24.14	0.1482	1.0007	0.4834	1.0001
MgK	0.00	0.00	0.0000	1.1991	0.2960	1.0004
SrL	2.35	1.47	0.0135	0.9638	0.5944	1.0012
LaL	51.25	20.26	0.4569	0.8792	1.0141	1.0000
Total	100.00	100.00				
(e) Chemical composition of secondary phase in LSGM1010						
OK	17.99	53.86	0.0712	1.2243	0.3280	1.0006
GaL	41.51	28.52	0.2544	0.9738	0.6289	1.0008
MgK	0.00	0.000	0.0000	1.1669	0.3337	1.0013
SrL	18.10	9.90	0.1101	0.9302	0.6534	1.0005
LaL	22.40	7.72	0.1919	0.8197	1.0083	1.0000
Total	100.00	100.00				
(f) Chemical composition of matrix phase in LSGM1010						
OK	19.07	58.68	0.0951	1.2374	0.4027	1.0004
GaL	33.80	23.86	0.1714	0.9840	0.5153	1.0001
MgK	0.00	0.00	0.0000	1.1791	0.3045	1.0004
SrL	3.62	2.03	0.0208	0.9443	0.6085	1.0010
LaL	43.51	15.42	0.3811	0.8621	1.0161	1.0000
Total	100.00	100.00				

TABLE III The quantitative XRD results of the secondary phases

Specimen	Secondary phase(%) LaSrGa3O7	LaSrGaO4
LSGM1005	2.7	0
LSGM1010	2.8	0
LSGM1015	6.4	0.5
LSGM1505	13.0	1.0
LSGM1515	7.1	0.8
LSGM1530	0	5.7
LSGM2005	10.6	0.6
LSGM2010	4.2	0.4
LSGM2020	0.8	0.9
LSGM2025	0	1.1
LSGM2520	1.0	1.2
LSGM2525	1.1	1.0

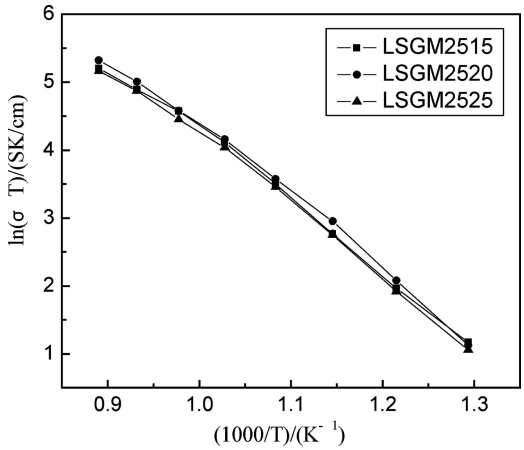

Figure 5 The conductivities of LSGM sintered at 1500°C for different time.

3.3. Microstructure

Typical back-scattered SEM micrographs of various composite LSGM are shown in Fig. 4. From Fig. 4a, it can be seen there existed long rod-like phase as secondary phase and granular-like matrix phase in LSGM0510 (shown with arrows). EDX analysis of rod-like phase and matrix phase are shown in Table IIa and b (Figure omitted), respectively. It can be seen that rod-like secondary phase is composed of $(La,Sr)_4Ga_2O_9$ and matrix phase is composed of (La,Sr) $(Ga,Mg)O_3$. But from XRD (see LSGM0510 in Fig. 1), it can be concluded that LSGM0510 is composed of only one phase-(La,Sr) $(Ga,Mg)O_3$ without secondary phase. This is probably because the small content of secondary phase can not be detected by XRD. This shows the limitation of phase-region diagram constructed only by XRD. From Fig. 4a–d, i.e. when x, Sr concentration $= 0.05$%mol and y, Mg concentration are increased, it can be seen that long rod phase disappeared gradually and equiaxed secondary phase

grow. From Fig. 4e, it can be seen that microstructures of LSGM1005 are composed of matrix phase and secondary phase (dark color), as shown with arrow. EDX analysis of matrix phase and second phase of LSGM1005 are shown in Table IIc and d (Figure omitted), respectively. From Table IIc and d, it can be seen that matrix phase is cubic perovskite-(La, Sr)(Ga, Mg)O_3 and secondary phase is $LaSrGa_3O_7$. It is correlated well with the XRD result shown in Fig. 1 (LSGM1005). From Fig. 4f, it can be seen that there existed matrix phase and polygonal phase as secondary phase, as shown with arrow. EDX diagrams of matrix phase and secondary phases of LSGM1010 are shown in Table IIe and f (Figure omitted), respectively. From Table IIe and f, it can be seen that polygonal secondary phase is $LaSrGa_3O_7$ and matrix phase is cubic perovskite (La,Sr)(Ga,Mg)O_3. It is correlated well with the XRD result shown in Fig. 1 (LSGM1010). Fig. 4e–h, i.e. when $x = 0.10\%$ mol and y are increased, it can be seen that there is a tendency, i.e. secondary phase grows from irregular phase into polygonal phase. From Fig. 4i–l, i.e. when $x = 0.15\%$ mol and y are increased, it can be seen that numbers of cavities are increased remarkably. From Fig. 4m–o, i.e., when $x = 0.20\%$ mol and y are increased, it can also be seen that cavities distribute at the interfaces of the matrix and secondary phases, the grain size is enhanced remarkably. From Fig. 4a–o, i.e., when x are fixed and y are increased, the grain size increases. The reason is maybe due to the increase of the strain energy caused by the addition of Mg. Fig. 4p also shows that there appears large grain size. From the works mentioned above, it can be concluded that with the increase of doped contents, i.e. $x + y$, the grain size increases.

By using quantitative XRD technique, the volume fractions of the secondary phases were shown in Table III. It should be pointed out that, in the SEM micrographs, the volume fractions of the secondary phases with large grains were greater than that of actual contents of the secondary phases (for example Fig. 4f) due to the selected area of photographing.

3.4. Ionic conductivity

Fig. 5 shows the conductivities of LSGM1520 samples sintered at 1500°C for different times under different testing temperature. It can be seen that, when sintering time changes from 6 to 24 h, conductivities increase, reach maximum then decrease with the further prolongation of sintering time. From Table I, it can be deduced that there is similar relationship between the relative densities and sintering time. It can be concluded that conductivities increase with the increase of the relative densities. This is because, with the increase of the relative densities, the cavities will be decreased and the resistance to conductivity caused by cavities will be decreased, therefore ionic conductivities will increase. The conductivities of LSGM with different Sr and Mg concentrations under different testing temperature are shown in Table IV. Ionic conductivity variation with concentration Sr and Mg of

TABLE IV Conductives of different composition LSGM under different testing temperature

	Conductivities under different testing temperature (S/cm)						
Sample	500°C	550°C	600°C	650°C	700°C	750°C	800°C
LSGM0505	9.0E-4	0.002	0.005	0.011	0.0209	0.034	0.050
LSGM0510	0.001	0.004	0.011	0.021	0.035	0.053	0.072
LSGM0515	0.002	0.007	0.017	0.032	0.054	0.081	0.110
LSGM0520	0.002	0.006	0.016	0.032	0.054	0.078	0.107
LSGM0525	0.003	0.007	0.014	0.026	0.046	0.070	0.092
LSGM0530	7.2E-4	0.002	0.006	0.015	0.027	0.046	0.070
LSGM1005	0.003	0.006	0.013	0.024	0.037	0.055	0.080
LSGM1010	0.002	0.006	0.014	0.027	0.052	0.080	0.114
LSGM1015	0.003	0.008	0.018	0.034	0.060	0.085	0.125
LSGM1020	0.002	0.007	0.017	0.033	0.057	0.092	0.127
LSGM1025	0.005	0.009	0.018	0.035	0.057	0.091	0.123
LSGM1030	0.001	0.004	0.010	0.018	0.035	0.057	0.092
LSGM1505	0.003	0.008	0.017	0.035	0.062	0.093	0.123
LSGM1510	0.003	0.008	0.018	0.036	0.062	0.093	0.130
LSGM1515	0.003	0.009	0.021	0.038	0.065	0.095	0.135
LSGM1520	0.003	0.008	0.018	0.036	0.067	0.105	0.148
LSGM1525	0.004	0.009	0.021	0.035	0.063	0.095	0.138
LSGM1530	0.002	0.005	0.013	0.027	0.048	0.074	0.106
LSGM2005	0.002	0.005	0.011	0.022	0.043	0.064	0.091
LSGM2010	0.001	0.004	0.010	0.025	0.048	0.087	0.130
LSGM2015	0.003	0.008	0.018	0.036	0.066	0.103	0.146
LSGM2020	0.004	0.009	0.021	0.036	0.063	0.101	0.134
LSGM2025	0.002	0.007	0.016	0.033	0.059	0.092	0.135
LSGM2510	0.002	0.006	0.012	0.024	0.045	0.067	0.095
LSGM2515	0.004	0.008	0.018	0.036	0.062	0.094	0.123
LSGM2520	0.0038	0.009	0.021	0.038	0.065	0.095	0.138
LSGM2525	0.003	0.008	0.017	0.034	0.058	0.083	0.121

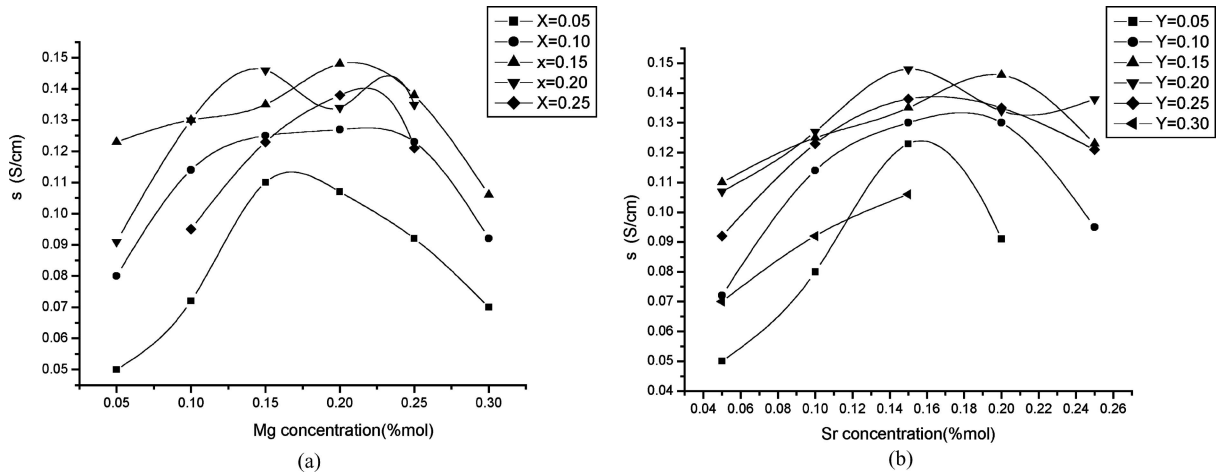

Figure 6 Ionic conductivity variation with concentration Sr and Mg of LSGM at 800°C (a) x, Sr concentration = constant, (b) y, Mg concentration = constant.

LSGM at 800°C are shown in Fig. 6. It can be seen that the ionic conductivities of LSGM increase with the increase of Sr addition or Mg addition firstly, and after reach maximum,then decrease. The optimized concentration in $La_{1-x}Sr_xGa_{1-y}Mg_yO_{3-0.5(x+y)}$ with the highest conductivity at 800°C ($\sigma = 0.148$ S/cm) is $x = 0.15\%$ mol, $y = 0.2\%$ mol i.e. corresponding to LSGM1520. At same time,it is noticed that LSGM2015 also has high conductivity at 800°C ($\sigma = 0.146$ S/cm). From Fig. 1, it can be seen that, at this two compositions, the samples remain a single-phase cubic (La, Sr)(Ga, Mg)O_3. This can explain the higher ionic conductivities of LSGM1520 and LSGM2015.

4. Conclusions

(1) The relative densities of samples depend on sintering time. With the prolongation of sintering time, the densities of samples prepared increase at first, reach a maximum and then decrease. With the increase of the relative densities of samples, the ionic conductivities increase.

(2) The ionic conductivities of LSGM increase with the increase of x, Sr concentration or y, Mg concentration at first, and after reach a maximum, the ionic conductivities of LSGM decrease with the increase of Sr concentration or Mg concentration. The optimized composition with high conductivity is LSGM1520 or LSGM2015. At this two compositions, the samples are composed of single phase-(La,Sr)(GaMg)O_3 without secondary phase.

(3) There exist regions of single-phase, two-phase or three-phase in various compositions of LSGM. Equiaxed, rode-like and polygonal secondary phases were examined by using SEM and EDX. With the increase of doped elements, i.e. $x + y$, the grain size increases.

(4) Owing to the limitation of XRD method, the phase-region diagram of LSGM with various concentrations of Sr and Mg constructed only from XRD is not accurate. In order to get LSGM with higher ionic conductivities, the phase-region diagram will be constructed more accurately. Many different testing ways will be used such as SEM, EDX, TEM, HRTEM, etc., in order to get more accurate phase diagram. The next work is expected to concentrate on constructing more accurate phase-region diagram.

Acknowledgments

The authors wish to acknowledge the financial support of this research by the Research Foundation of Educating Chinese People coming back from abroad and the Max-Planck-Society, Germany.

References

1. N. M. SAMMER, G. A. TOMPSETTE, R. J. PHILLIPS, *et al. Solid State Ionics* **111** (1998) 1.
2. G. DOTELLI, I. N. SORA, C. SCHMID, *et al., Solid State Ionics* **152/153** (2002) 509.
3. X. J. CHEN, K. A. KHOR, S. H. CHAN, *et al., Mater. Sci. Eng. A* **335** (2002) 246.
4. T. HORITA, H. NEGISHI, K. YAMAJI, *et al., Electrochimica Acta* **46** (2001) 1837.
5. T. ISHIHARA, T. SHIBAYAMA, H. NISHIGUCHI, *et al., J. Mater. Sci.* **36** (2001) 1125.
6. A. B. STAMBOULI and E. TRAVERSA, *Renewable and Sustainable Energy Review* **6** (2002) 433.
7. K. HUANG, J. WAN and J. B. GOODENOUGH, *J. Mater. Sci.* **36** (2001) 1093.
8. K. CHOY, W. BAI, S. CHAROJROCHKUL, *et al., J. Power Sourc.* **71** (1998) 361.
9. T. ISHIHARA, H. MATSUDA and Y. TAKITA, *J. Am. Chem. Soc.* **116** (1994) 3801.
10. M. FENG and J. B. GOODENOUGH, *Euro. J. Solid State Inorg. Chem.* **31** (1994) 663.
11. T. ISHIHARA, H. MATSNDA and Y. TAKITA, *Solid State Ionics* **113–115** (1998) 571.
12. T. MATHEWS, J. R. SELLAR and B. C. MUDDLE, *Chem. Mater.* **12** (2002) 917.
13. T. MATHEWS and J. R. SELLAR, *Solid State Ionics* **135** (2000) 411.
14. O. SCHULZ and M. MARTIN, *J. Am. Chem. Soc.* **116** (1994) 3801.
15. S. M. CHOI, K. T. LEE, S. KIM, *et al., Solid State Ionics* **131** (2000) 221.

16. E. DJURADO and M. LABEAU, *J. Euro.Ceram. Soc.* **18** (1998) 1397.
17. K. HUANG, M. FENG and J. B. GOODENOUGH. *J. Am. Ceram. Soc.* **79** (1996) 1100.
18. A. TARANCON, G. DEZANNEAU, J. ARBIOL, F. PEIRO and J. R. MORANTE, *J. Power Sources* **118** (2003) 256.
19. L. G. CONG, T. M. HE, Y. JI, P. G. GUAN, Y. L. HUANG and W. H. SU, *J. Alloys Comp.* **348** (2003) 325.
20. S. BASKARAN, C. A. LEWINSOHN, Y.-S. CHOU, M. QIAN, J. W. STEVENSON and T. R. ARMSTRONG, *J. Mater. Sci.* **34** (1999) 3913.
21. I. YASUDA, Y. MATSUZAKI, T. YAMAKAWA and T. KOYAMA. *Solid State Ionics* **135** (2000) 381.
22. K. HUANG, R. S. TICHY and J. B. GOODENOUGH, *J. Am. Ceram. Soc.* **81** (1998) 2565.
23. K. HUANG, R. S. TICHY and J. B. GOODENOUGH, *J. Am. Ceram. Soc.* **81** (1998) 2576.
24. K. HUANG, R. S. TICHY and J. B. GOODENOUGH, *J. Am. Ceram. Soc.* **81** (1998) 2581.
25. M. LERCH, H. BOYSEN and T. HANSEN, *J. Phys. Chem. Solids* **62** (2001) 445.
26. W. H. YAO, Z. L. TANG, Z. T. ZHANG, S. H. LUO, J. LI and Q. Q. TAN, *Mater. Sci. Eng. B* **99** (2003) 309.
27. K. YAMAJI, H. NEGISHI, T. HORITA, *et al*., *Solid State Ionics* **135** (2000) 389.

Received 27 January
and accepted 23 August 2005